SCIENTIFIC REPORTS

OPEN

SUBJECT AREAS:
SYNTHESIS AND PROCESSING
STRUCTURAL PROPERTIES

Received
31 January 2014

Accepted
1 May 2014

Published
21 May 2014

Correspondence and requests for materials should be addressed to C.S.B. (elebcs@nus.edu.sg)

Probing the Role of an Atomically Thin SiN_x Interlayer on the Structure of Ultrathin Carbon Films

Neeraj Dwivedi[1], Ehsan Rismani-Yazdi[1], Reuben J. Yeo[1], Partho S. Goohpattader[1], Nalam Satyanarayana[1], Narasimhan Srinivasan[2], Boris Druz[2], S. Tripathy[3] & C. S. Bhatia[1]

[1]Department of Electrical and Computer Engineering, National University of Singapore, Singapore 117583, [2]Veeco Instruments Inc, Terminal Drive Plainview, New York 11803, United States, [3]Institute of Materials Research and Engineering (IMRE), A*STAR (Agency for Science, Technology, and Research), 3 Research Link, Singapore 117602.

Filtered cathodic vacuum arc (FCVA) processed carbon films are being considered as a promising protective media overcoat material for future hard disk drives (HDDs). However, at ultrathin film levels, FCVA-deposited carbon films show a dramatic change in their structure in terms of loss of sp^3 bonding, density, wear resistance etc., compared to their bulk counterpart. We report for the first time how an atomically thin (0.4 nm) silicon nitride (SiN_x) interlayer helps in maintaining/improving the sp^3 carbon bonding, enhancing interfacial strength/bonding, improving oxidation/corrosion resistance, and strengthening the tribological properties of FCVA-deposited carbon films, even at ultrathin levels (1.2 nm). We propose the role of the SiN_x interlayer in preventing the catalytic activity of Co and Pt in media, leading to enhanced sp^3C bonding (relative enhancement ~40%). These findings are extremely important in view of the atomic level understanding of structural modification and the development of high density HDDs.

Ultrathin diamond-like carbon (DLC) films are widely used in the hard disk drives (HDDs) industry to protect the surface of hard disk media and head from corrosion and mechanical wear[1–4]. With the continuously increasing demands of inexpensive and small HDDs[5], the areal density of these drives is increasing at a rate of 20–30% annually[6]. The reduction of magnetic spacing, which is the vertical distance between the magnetic layer in media and magnetic elements in the head, is one of the most important parameters to achieve high areal density as Wallace[7] had proposed that the readback signal increases exponentially with decreasing magnetic spacing. It has been reported that a carbon overcoat (COC) of ~2.5 nm is required[6] to obtain an areal density of ~1 Tb/in^2. In order to advance beyond 1 Tb/in^2, the COC thickness has to be reduced. Currently, plasma enhanced chemical vapor deposition (PECVD) grown hydrogenated carbon (CH_x) overcoats (OCs) are used on commercial media disks[8,9]. However, the reduction of the current commercial COCs thickness below 2 nm may introduce many corrosion and tribological challenges. Recently, heat-assisted magnetic recording (HAMR) – which employs a highly focused and intense laser beam to help lower the coercivity, momentarily, of the media to allow recording of information on it – has gained enormous scientific and industrial attention for future high density HDDs[8,9]. Since the laser beam also interacts with COC, the performance of current commercial COC is degraded due to its thermal instability[8,9]. In order to obtain better corrosion and wear protection at low COC thicknesses while keeping HAMR application in mind, alternative techniques for the development of COC on media have to be explored.

The FCVA technique, which has the ability to produce highly dense and continuous carbon films even at a thickness level of ~2 nm[10,11], has opened up possibilities for creating next generation high areal density HDDs. It produces a highly ionized (~90%) plasma of carbon ions which have an average energy of ~20–25 eV[4]. These carbon ions strike the substrate and produce a smooth, continuous, highly dense and high sp^3 bonded carbon film[4]. The continuous and dense structure of FCVA-deposited carbon films is important for protecting the magnetic hard disk media against corrosion/oxidation, while the high sp^3 carbon (sp^3C) bonding characteristic within the film offers excellent resistance against mechanical wear. Moreover, given its high thermal stability property, FCVA-deposited carbon has been considered as an ideal COC for HAMR application[8,9,11].

However, it has been reported that a reduction of the thickness of FCVA-deposited carbon also introduces dramatic structural changes, such as lowering the sp^3C bonding as compared to its bulk counterpart. Robertson[4] and Chhowalla *et al.*[12] suggested that thicker carbon films of 50 nm and above grown using FCVA (also referred

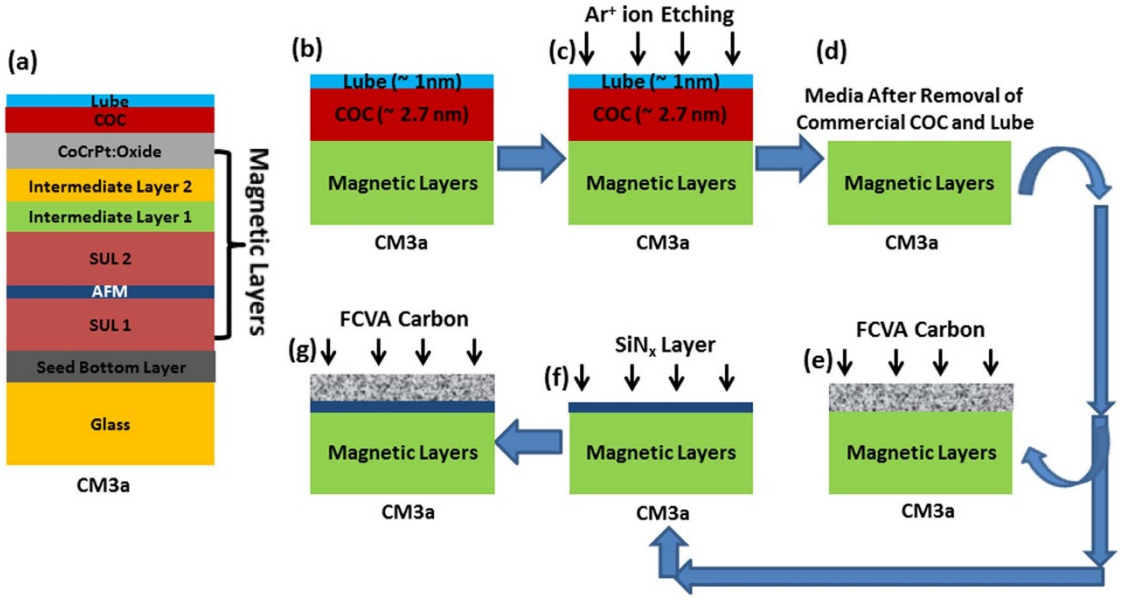

Figure 1 | Schematic representation of the substrate and deposition process. (a) Cross-sectional schematic view of commercial magnetic media (CM3a) with several magnetic layers, commercial COC and lubricant, (b) simplified structure of CM3a, (c) Ar^+ ion etching of CM3a to remove the commercial COC and lube, (d) CM3a media after removal of commercial COC and lube, (e) deposition of carbon films by FCVA on etched CM3a, (f) deposition of atomically thin SiN_x layer on etched CM3a, and (g) deposition of carbon films on the SiN_x layer on top of etched CM3a by FCVA.

to as tetrahedral amorphous carbon or ta-C) could have high sp^3C bonding in the range of ~80–90%. However, Zhang and Komvopoulos[2] have observed sp^3C bonding in the range of ~20–50% in FCVA carbon modified hard disk media samples, where the carbon film thickness was only ~2–3 nm. Beghi *et al.*[13] performed in-depth investigations of the bonding of FCVA-grown carbon films as a function of thickness and found that both sp^3 bonding and density were reduced with decreasing thickness below ~10 nm. Still, Ferrari[14] suggested that FCVA-deposited carbon films could have sp^3C bonding of ~50% even at a thickness of 2 nm, which is considerably higher than sputtered and PECVD-based carbon films of the same thickness. As next generation high density HDDs require COCs with thickness of 1–2 nm or even less with their high thermal stability and protective characteristics, FCVA-deposited carbon seems to be a potential candidate as a COC for future HDDs. However, its structural properties – mainly the sp^3C bonding at the thickness level of 1 to 2 nm – have to be maintained or improved. Hence, new approaches, processes and structural designs of media disk OCs have to be proposed and executed.

Silicon nitride (SiN_x) has a high atomic density and is being considered in the magnetic storage industry as an alternative material for COC on media[15,16]. However, as a single overcoat, SiN_x suffers from poor tribological performance and oxidation[15,16]. Nevertheless, when used together, the SiN_x and FCVA-deposited carbon in one structure may show promising properties due to their synergistic effect. Recently, Bunnak *et al.*[17,18] prepared composite SiN_x/DLC films by the FCVA (for DLC) and radio frequency (RF) sputtering (for SiN_x) techniques, and found that SiN_x/DLC films revealed better structural and mechanical properties than single-layer DLC. However, their work investigated ~10 nm thick films, which is far beyond the current thickness requirement of COC on magnetic storage media. Hence, the grand challenge is to maintain the better structural properties of FCVA-deposited carbon at the thickness of 1–2 nm.

In this work, we explore the structural properties of ultrathin carbon films grown with and without the silicon nitride (SiN_x) interlayer. The understanding of how the application of an atomically thin SiN_x (0.4 nm) interlayer influences the interfacial bonding and structure of ultrathin carbon films lies at the core of this study. Given their ability to probe the structure of ultrathin DLC films, Raman spectroscopy and X-ray photoelectron spectroscopy (XPS)[2–4,8–12,17,18] are employed as spectroscopic characterization tools for structural analysis.

Results

Fig. 1a displays the cross-sectional schematic of a 2.5″ commercial hard disk media (CM3a) sample used in this work. A commercial hard disk typically contains a seed layer grown on a glass substrate, above which many magnetic layers are deposited, such as the soft underlayer 1 (SUL 1), antiferromagnetic (AFM) coupling layer, SUL 2, intermediate layer 1, intermediate layer 2, and finally, the magnetic storage layer of CoCrPt:Oxide on top. Above the magnetic storage layer, a ~2.7 nm thick layer of commercial COC followed by a ~1 nm lubricant (lube) layer are deposited to protect the magnetic media from corrosion and wear. Figs. 1b–1g schematically illustrates the deposition process of the ultrathin FCVA-based carbon films with and without the SiN_x interlayer. To grow these films, the commercial COC and lube had to be removed first. Hence, the etching of commercial COC and lube of CM3a was conducted in an ion beam etch chamber using Ar^+ ions at ion energy of 300 eV (Figs. 1c and 1d), followed by the transferring of the etched CM3a samples in the FCVA chamber under high vacuum conditions. The reason for applying this etching step of *in-situ* overcoat removal is to perform the growth of carbon films on an oxide-free surface of magnetic media. The deposition of ultrathin carbon films was done on etched hard disk media samples using the FCVA process.

Two runs were performed on two separate batches of the samples after etching to obtain single-layer FCVA-deposited carbon films of thicknesses ~1.2 nm (CM3a/12C) and ~1.6 nm (CM3a/16C) (Fig. 1e). A third run was performed to fabricate the SiN_x/carbon bilayer structure (CM3a/4SiN12C) with SiN_x as an interlayer. An atomically thin SiN_x layer of ~0.4 nm was first deposited on the etched media surface using pulsed direct current (DC) reactive sputtering of Si target with a gaseous mixture of Ar and N_2 (Fig. 1f), followed by the deposition of a ~1.2 nm carbon film by FCVA (Fig. 1g). The description of all the samples used in this work is given in Table 1.

Transmission electron microscopy (TEM). The thicknesses of the FCVA-deposited carbon films with and without the SiN_x interlayer

Table 1 | Nomenclature and description of different samples used in present work

Nomenclature	Sample Description
CMb	Specially prepared commercial magnetic media disk without COC and lube.
CMC	Specially prepared commercial magnetic media disk with its original COC (~2.7 nm) but no lube.
CM3a/12C	Overcoats etched CM3a containing ultrathin a-C film (~1.2 nm) grown using FCVA.
CM3a/16C	Overcoats etched CM3a containing ultrathin a-C film (~1.6 nm) grown using FCVA.
CM3a/4SiN12C	Overcoats etched CM3a containing atomically thin SiN_x interlayer (0.4 nm) by pulsed DC reactive sputtering, followed by deposition of ultrathin a-C film (~1.2 nm) using FCVA.

as well as the specially prepared commercial media sample with commercial COC but no lube (sample CMC) were measured using high resolution cross-section TEM, as shown in Figs. 2a–2d. The thicknesses of the different OCs can be estimated between the capping layer and the magnetic layers. It is evident from Fig. 2a that the thickness of commercial COC in sample CMC was found to be 2.7 ± 0.1 nm. On the other hand, the thicknesses of the FCVA-deposited carbon films in samples CM3a/12C and CM3a/16C (Figs. 2b and 2c) were measured to be ~1.2 ± 0.1 nm and ~1.6 ± 0.1 nm, respectively, which matched with our calibration. Lastly, the OC thickness in sample CM3a/4SiN12C was also measured to be ~1.6 ± 0.1 nm. Due to the similar contrast of SiN_x and carbon observed in the TEM image, coupled with the atomic level thickness (~0.4 nm) of SiN_x which could possibly have been intermixed with carbon, it is difficult to distinguish between the two layers from the TEM cross-sectional image of this sample in Fig. 2d. However, the angle resolved X-ray photoelectron spectroscopy (ARXPS) results (discussed later) revealed the presence of the SiN_x interlayer in the CM3a/4SiN12C sample. The thickness of the overcoats measured by TEM matches well with the calibrated deposition rate, which was carried out by X-ray reflectivity (XRR) measurements. Details are given in the methods section.

Further, while analyzing the TEM images, we found that FCVA-deposited carbon in sample CM3a/12C showed a formation of nanocrystalline layered structure. The 1.2 nm COC comprised few atomic layers and deposited onto the CoCrPt-alloys based media. The Co and Pt, which are transition metals, are active catalyst and may assist to form the nanostructured morphology in carbon due to catalytic activity. These nanostructures may be rich in sp^2 bonding and clustering, thus this sample should possess relatively lesser sp^3 bonding, which as explained in discussion section. However, the layered structure was relatively reduced in samples CM3a/16C and CM3a/4SiN12C. This may be due to the increase in sp^3 bonding and reduction in the catalytic activity of the Co and Pt atoms because of an increase in the carbon thickness and introduction of 0.4 nm SiN_x interlayer respectively, which are explained in discussion section. In contrast, lesser or negligible layering of carbon was observed in a TEM image of sample CMC.

Angle resolved X-ray photoelectron spectroscopy (ARXPS). ARXPS, utilizing different grazing angles for surface analysis, can effectively probe the chemical bonding and structure of ultrathin films and interfaces. Hence, detailed analyses of the chemical structure, composition and oxidation/corrosion resistance of these samples were performed using ARXPS. Each of the high resolution spectra was recorded under varied photoelectron take-off angles (TOA) from 15° to 65° (90° being normal to the surface). Figs. 3a–3c show the C 1s, Co $2p_{3/2}$ and Cr 2p core level spectra of sample CM3a/12C, while Figs. 3d–3h display the C 1s, Co $2p_{3/2}$, Cr 2p Si 2p and N 1s core level spectra of sample CM3a/4SiN12C. At a TOA of 15°, the signal came mainly from the topmost surface giving a strong C 1s peak, and weaker Co $2p_{3/2}$ and Cr $2p_{3/2}$ or Cr $2p_{1/2}$ peaks in samples CM3a/12C and CM3a/4SiN12C. The intensity of the Co $2p_{3/2}$ and Cr $2p_{3/2}$ peaks in both of these samples as well as the intensity of the Si 2p and N 1s peaks in sample CM3a/4SiN12C were found to rise continuously with increasing TOA from 15° to

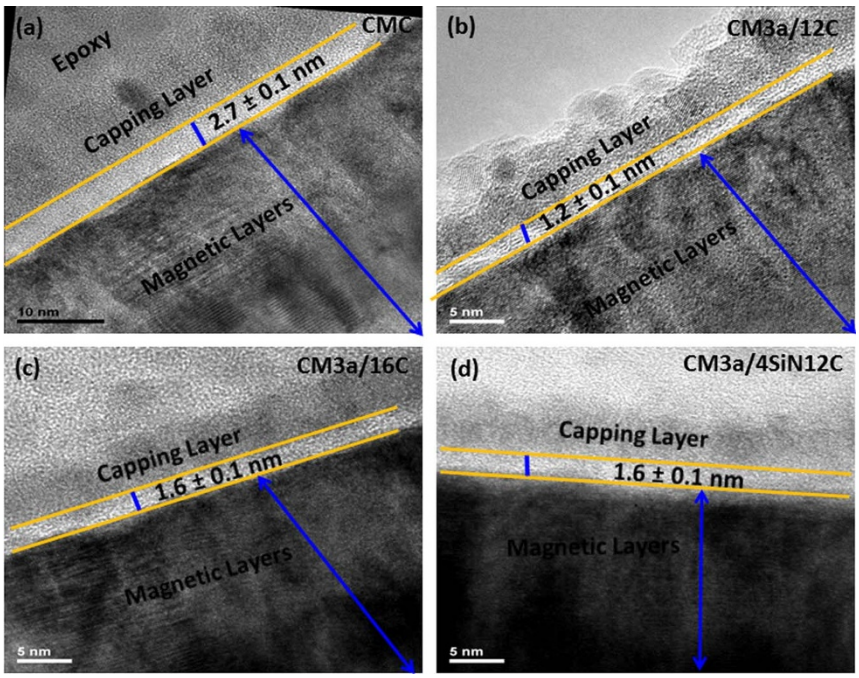

Figure 2 | Cross-sectional TEM analysis for determination of the thickness and the structure of carbon films. TEM images of samples (a) CMC, (b) CM3a/12C, (c) CM3a/16C and (d) CM3a/4SiN12C.

65°. This is due to the TOA having a steeper angle with respect to the surface as the angle increases, which analyzes the photoelectrons that are emitted deeper beneath the surface, nearer to the interface and media. This relation, however, does not hold for the C 1s core level spectra. With increasing TOA from 15° to 25°, the intensity of the C 1s peak for both spectra rose due to a high carbon signal from the surface, but beyond TOA of 25°, no relation between the intensity of the C 1s peak and TOA was observed as the TOA approached the interface and media. Since the C 1s peak positions at the lowest and highest TOAs of 15° and 65° were found to be almost at the same binding energy position and the maximum intensities of the Co $2p_{3/2}$ and Cr $2p_{3/2}$ peaks were observed at TOA of 65°, the spectra corresponding to the TOA of 65° were considered for detailed structural, compositional and oxidation analyses of both samples. Moreover, the XPS spectra of samples CMC and CM3a/16C (not given in Fig. 3) were also recorded at a TOA of 65° ± 2° for analysis and comparison. Additionally, it should be noted that the Si and N peaks (shown in Figs. 3g and 3h) became prominent at TOA of 35° as compared to 15° and 25°, due to the higher probability of escaping photoelectrons close to the interface region at this TOA. Hence, the Si 2p and N 1s spectra taken at TOA of 35° were also considered for interface bonding and other analyses, apart from their spectra at TOA of 65°.

The Co $2p_{3/2}$ spectra of samples CMb, CMC, CM3a/12C, CM3a/16C and CM3a/4SiN12C are compared in Figs. 4a–4e, whereas their Cr $2p_{3/2}$ spectra are compared in Figs. 4f–4j. Sample CMb was specially prepared bare magnetic media with a magnetic storage layer of CoCrPt-oxide on top (i.e. no COC and no lube). It is evident from Fig. 4a that CMb showed a very minor peak at ~778.1 eV corresponding to the metallic state of Co, but a very broad and intense major peak at ~780.5 eV assigned to the oxide state of Co[2]. This implies that Co in CMb without any surface protection exists mainly in the oxidized state[2]. Similarly, the Cr $2p_{3/2}$ peak in CMb centered at ~576.0 eV was found to be very broad, indicating that Cr also exists mainly in the oxidized state. When OCs were deposited over the magnetic media, the Co $2p_{3/2}$ and Cr $2p_{3/2}$ peaks were observed at ~778.1 eV and ~574.0 ± 0.2 eV respectively, in samples CMC, CM3a/12C, CM3a/16C and CM3a/4SiN12C. This indicated that all the OCs, whether the thicker commercial COC (~2.7 nm) or thinner OCs with FCVA-deposited carbon, provide protection against oxidation/corrosion for the underlying magnetic storage layer. It is interesting to note that FCVA-deposited carbon, even at the thickness levels of 1.2 nm and 1.6 nm with and without the SiN_x interlayer, provides considerably higher protection against oxidation/corrosion.

In order to examine the interfacial and bulk bonding of various elements, the C 1s, Co $2p_{3/2}$, Cr $2p_{3/2}$, Si 2p and N 1s core level spectra of various samples taken at TOA of 65° were analyzed and compared in Figs. 5a–5n. The C 1s spectra of samples CMC, CM3a/12C, CM3a/16C, and CM3a/4SiN12C were fitted with four to five Gaussian components (Figs. 5a–5d), the Co $2p_{3/2}$ spectra were fitted with four to five Lorentzian-Gaussian components (Figs. 5e–5h), and the Cr $2p_{3/2}$ spectra were fitted with five Gaussian components (Figs. 5i–5l). The C 1s core level spectra of all samples showed four peaks #1, #2, #3

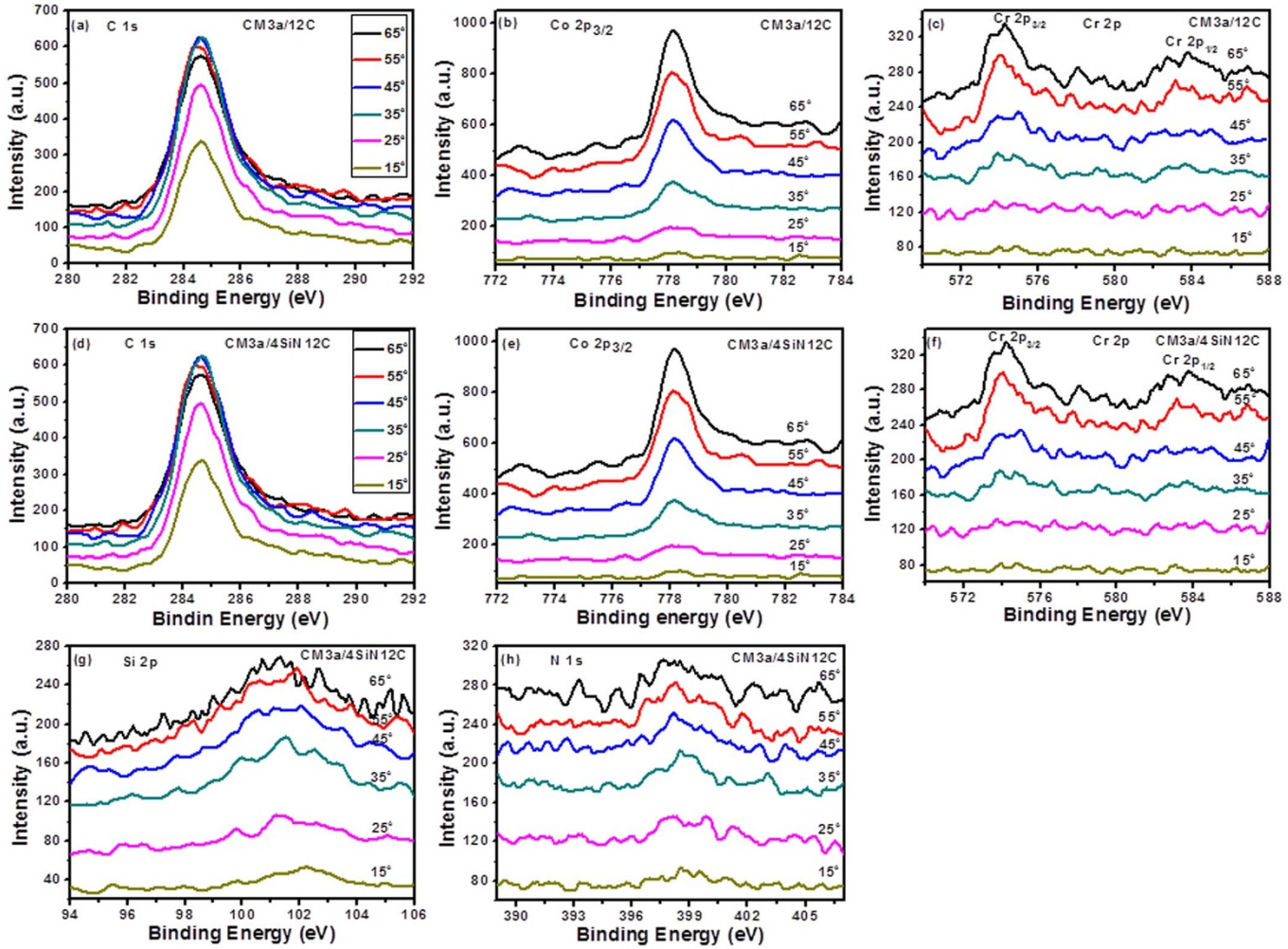

Figure 3 | ARXPS analysis. XPS core level spectra of (a) C 1s, (b) Co $2p_{3/2}$ and (c) Cr 2p for sample CM3a/12C; and (d) C 1s, (e) Co $2p_{3/2}$, (f) Cr 2p, (g) Si 2p and (h) N 1s for sample CM3a/4SiN12C recorded at TOA from 15° to 65°.

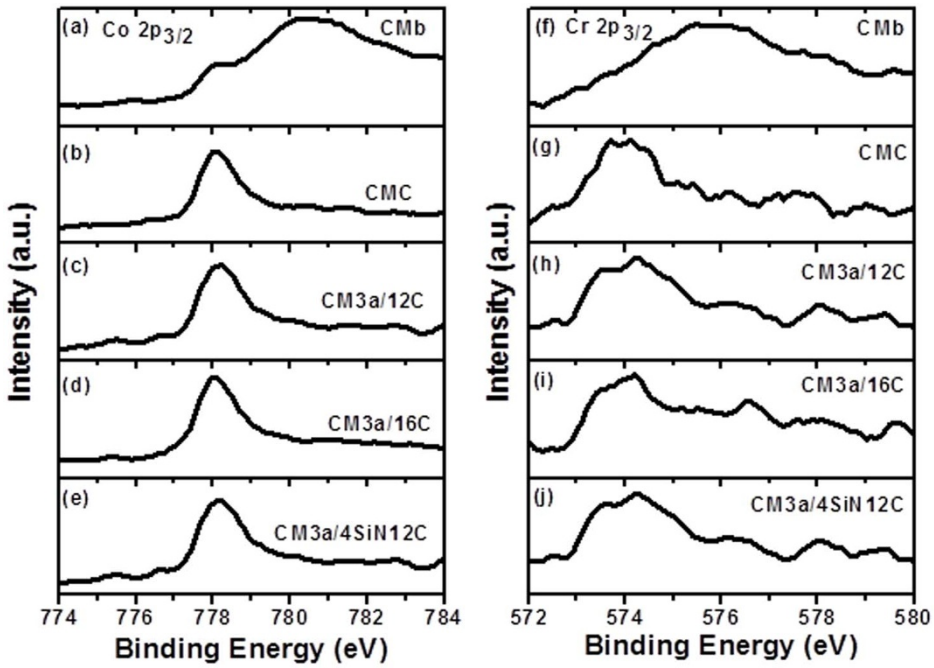

Figure 4 | Revealing the extent of oxidation/corrosion of Co and Cr in CMb and improvement of oxidation/corrosion resistance after application of COCs. The XPS core level spectra of (a)–(e) Co $2p_{3/2}$ and (f)–(j) Cr $2p_{3/2}$ for samples CMb, CMC, CM3a/12C, CM3a/16C and CM3a/4SiN12C recorded at TOA of 65°.

and #4 at 284.1 ± 0.1 eV, 284.9 eV, 286.2 ± 0.1 eV and 287.9 ± 0.1 eV, respectively, assigned to sp^2C, sp^3C, C–O and C = O bonding, respectively[2,19–21]. In addition, a fifth peak (#5) was observed only in CM3a/4SiN12C at ~283.0 eV, which corresponds to Si-C bonding[17,18,21]. Similarly, the Co $2p_{3/2}$ core level spectra of all samples showed four peaks #1, #2, #3 and #4 at 778.0 ± 0.1 eV, 779.2 ± 0.1 eV, 780.3 ± 0.3 eV and 781.5 ± 0.2 eV, respectively, which can be attributed to Co-Co (metallic cobalt), Co-oxide (cobalt oxide as in Co_2O_3), Co-oxide/hydroxide (such as CoO, Co_3O_4, CoOOH or $Co(OH)_2$) and Co-oxide/hydroxide (such as CoO, Co_3O_4, $Co(OH)_2$), respectively[21–24]. Again, a fifth peak (#5) was observed only in CM3a/4SiN12C at ~778.5 eV, which corresponds to Co-Si bonding[21,25]. The Cr $2p_{3/2}$ core level spectra showed five peaks. Peaks #1 and #2 were found at 573.7 ± 0.1 eV and 574.3 ± 0.1 eV, respectively, both of them corresponding to Cr-Cr bonding (metallic Cr). Peaks #4 and #5 were observed at 576.2 ± 0.4 eV and 577.8 ± 0.3 eV, which can be attributed to Cr-oxide and Cr-oxide/hydroxide, respectively[22,24,26,27]. Due care was taken in analyzing peak #3. In samples CMC and CM3a/16C, peak #3 was observed at 575.2 ± 0.1 eV, which is ascribed to Cr-Cr bonding, whereas in samples CM3a/12C and CM3a/4SiN12C, peak #3 was obtained at 574.9 eV. For sample CM3a/12C, this peak corresponds to Cr-Cr bonding. However, for sample CM3a/4SiN12C, peak #3 may also have some contribution from Cr_2N bonding at the interface in addition to Cr-Cr bonding[28]. The reason for fitting two to three peaks ascribing to Cr-Cr bonding only was to get the best fit to the data.

In order to examine interfacial bonding, the Si 2p and N 1s core level spectra of sample CM3a/4SiN12C taken at TOA of 65° and 35° were fitted with various Gaussian components. For the spectra recorded at 65°, the Si 2p and N 1s spectra were fitted with four and five Gaussian components, respectively, whereas these spectra were fitted with five and seven Gaussian components, respectively, when the spectra was recorded at 35°. The difference in number of fitting components was due to the slight difference in shape of the spectra observed at 65° and 35°, which may be due to the difference in the escape depth of the photoelectrons.

Figs. 5m and 5n show the Si 2p and N 1s core level spectra of sample CM3a/4SiN12C taken at TOA of 65°. The Si 2p core level spectrum revealed four constituent peaks #1, #2, #3 and #4 at 99.4 eV, 100.6 eV, 101.5 eV and 102.8 eV respectively, ascribed to Si-Si, Si-C, Si-N and Si-O/Si-N-O bonding, respectively[17,21,29]. On the other hand, the N 1 s spectrum showed five constituent peaks in which three peaks #1, #2, and #3 at 397.7 eV, 398.9 eV and 400.4 eV were attributed to Si-N, sp^3C-N and sp^2C-N bonding, respectively[29,30]. However, peaks #4 and #5 were found at 402.4 eV and 403.7 eV respectively, corresponding to NO_x bonding[31]. We have also deconvoluted and analyzed the Si 2p and N 1s core level spectra recorded at TOA of 35° with five and seven Gaussian components to obtain the best fit to the data, as shown in Figs. 5o and 5p. Out of these five peaks, four peaks in the Si 2p spectrum were similar to that observed at TOA of 65° but with a slight change in their peak positions. The additional peak #5 in the Si 2p spectrum recorded at TOA of 35° was found to be at 103.3 eV, which is assigned to Si = O bonding[17]. Likewise, out of the seven peaks in the N 1s core level spectrum, five peaks were similar to those observed at TOA of 65° but with a small shift in their peak positions. Additionally, a fifth peak (#5), which was obtained at 403.1 eV, can be assigned to NO_x/N-N bonding[31,32]. The N 1s spectrum recorded at TOA of 35° showed two additional peaks: #6 and #7 at 397.4 eV and 401.1 eV, respectively. Peak #6 corresponds to Cr_2N bonding[33] while peak #7 seems to have the same type of bonding as peak #3, which is sp^2C-N bonding.

The percentages of the constituent peaks in all the core level spectra obtained for all samples were determined by an area ratio method and are shown in Fig. 6. The total sp^3C bonding in samples CMC and CM3a/12C was found to be ~33% in both; however, it continuously increased to ~37% and ~46.3% in samples CM3a/16C and CM3a/4SiN12C, respectively. Comparing the sp^3C bonding of sample CM3a/4SiN12C with sample CM3a/16C (while keeping total thickness constant at ~1.6 nm), an absolute increase of ~9.3% (relative increase of ~25%) in sp^3C bonding was observed in sample CM3a/4SiN12C. Similarly, comparing the sp^3C bonding of sample CM3a/4SiN12C with sample CM3a/12C (while keeping the carbon thickness constant at ~1.2 nm), an absolute increase of ~13.3% (relative increase of ~40%) in sp^3C bonding was observed in sample CM3a/4SiN12C. The increase in sp^3C bonding can thus be related to a SiN_x-induced change in the structure of the FCVA-deposited carbon film.

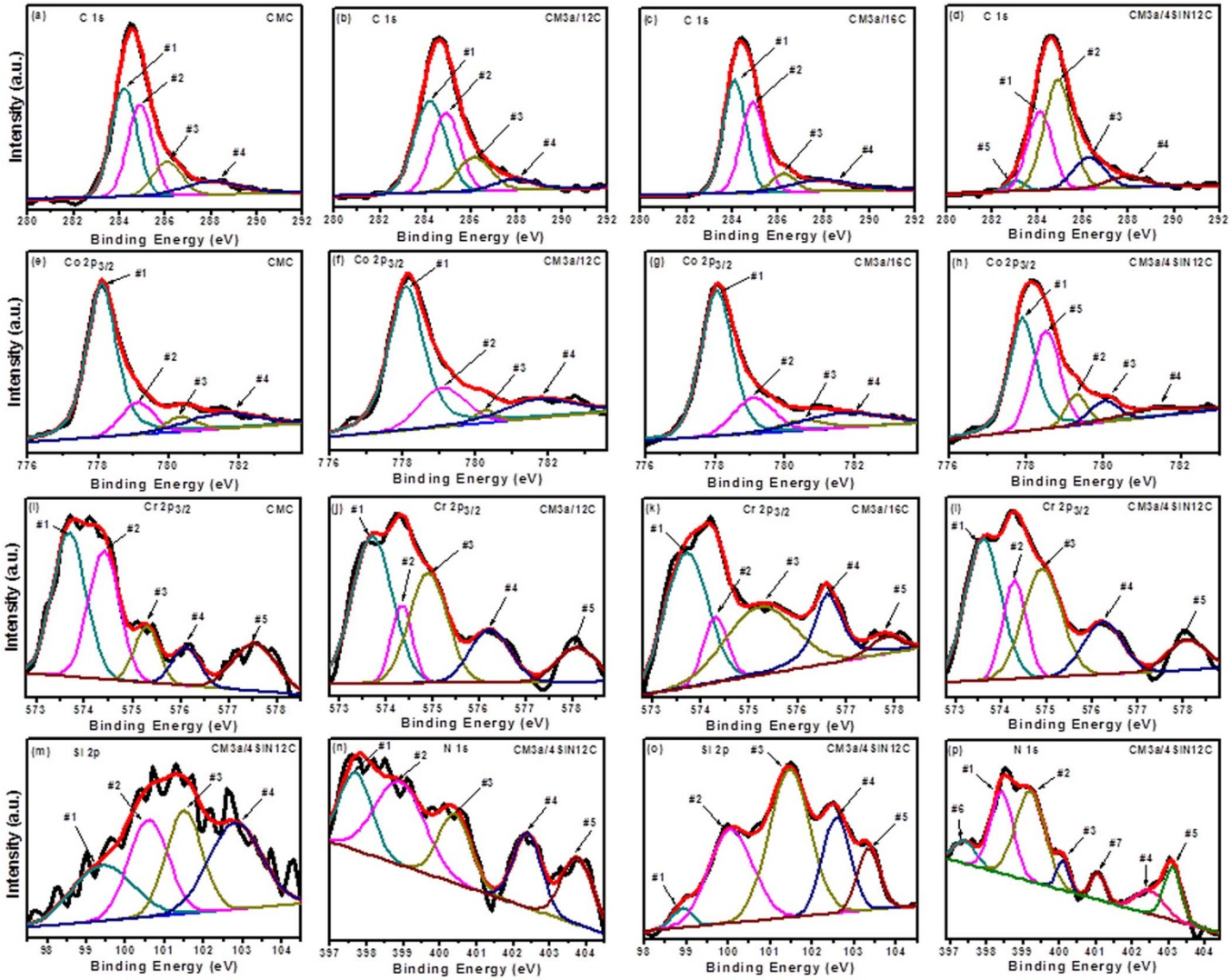

Figure 5 | Evaluation of carbon bonding, interfacial bonding and quantitative analysis of oxidation/corrosion protection of the media layer. Deconvolution of the core level spectra of (a)–(d) C 1s, (e)–(h) Co $2p_{3/2}$, and (i)–(l) Cr $2p_{3/2}$ for samples CMC, CM3a/12C, CM3a/16C and CM3a/4SiN12C recorded at TOA of 65°. Deconvolution of core level spectra of (m) Si 2p and (n) N 1s recorded at TOA of 65°, and (o) Si 2p and (p) N 1s recorded at TOA of 35° for sample CM3a/4SiN12C.

From the Co $2p_{3/2}$ core level spectra, the metallic Co-Co/Co-Si (Co oxide/hydroxide) bonding fractions in samples CMC, CM3a/12C, CM3a/16C and CM3a/4SiN12C were also estimated and found to be ~68% (~32%), ~63% (~37%), ~62% (~38%) and ~78% (~22%), respectively. Likewise, from the Cr $2p_{3/2}$ core level spectra, Cr-Cr/Cr_2N (Cr oxide/hydroxide) bonding fractions in these samples were found to be ~76% (~24%), ~77% (~23%), ~79% (~21%) and ~79% (~21%), respectively. These findings indicate that the introduction of an atomically thin SiN_x interlayer in carbon helps in enhancing (lowering) its sp^3C (sp^2C) bonding, reducing Co oxidation and maintaining/reducing Cr oxidation, as compared to carbon films without a SiN_x interlayer and thicker commercial COC. The details of the peak positions, associated bonding and the percentages of the constituent peaks of all the core level spectra obtained for all the samples are summarized in Table S1.1–S1.6 under supplementary information.

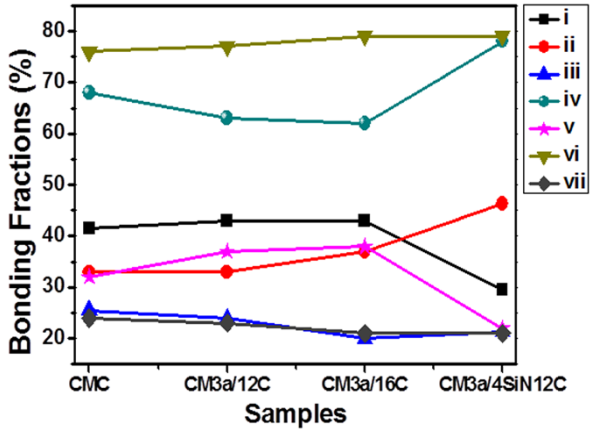

Figure 6 | Quantitative analysis of various carbon bonding and oxidation/corrosion levels of Co and Cr. Variations of i: sp^2C bonding, ii: sp^3C bonding, iii: bonding states of C with O (both C–O and C = O), iv: Co metallic/silicide bonding, v: Co (oxide/hydroxide) bonding, vi: Cr metallic/nitride bonding, and vii: Cr (oxide/hydroxide) bonding for samples CMC, CM3a/12C, CM3a/16C and CM3a/4SiN12C.

Micro-Raman Spectroscopy. Raman spectroscopy is a very promising tool for structural characterization of DLC films. The visible (488 nm) and ultraviolet (UV, 325 nm) Raman spectra of samples CMC, CM3a/12C, CM3a/16C and CM3a/4SiN12C are shown in Figs. 7a–7h. The Raman spectra of all samples were fitted

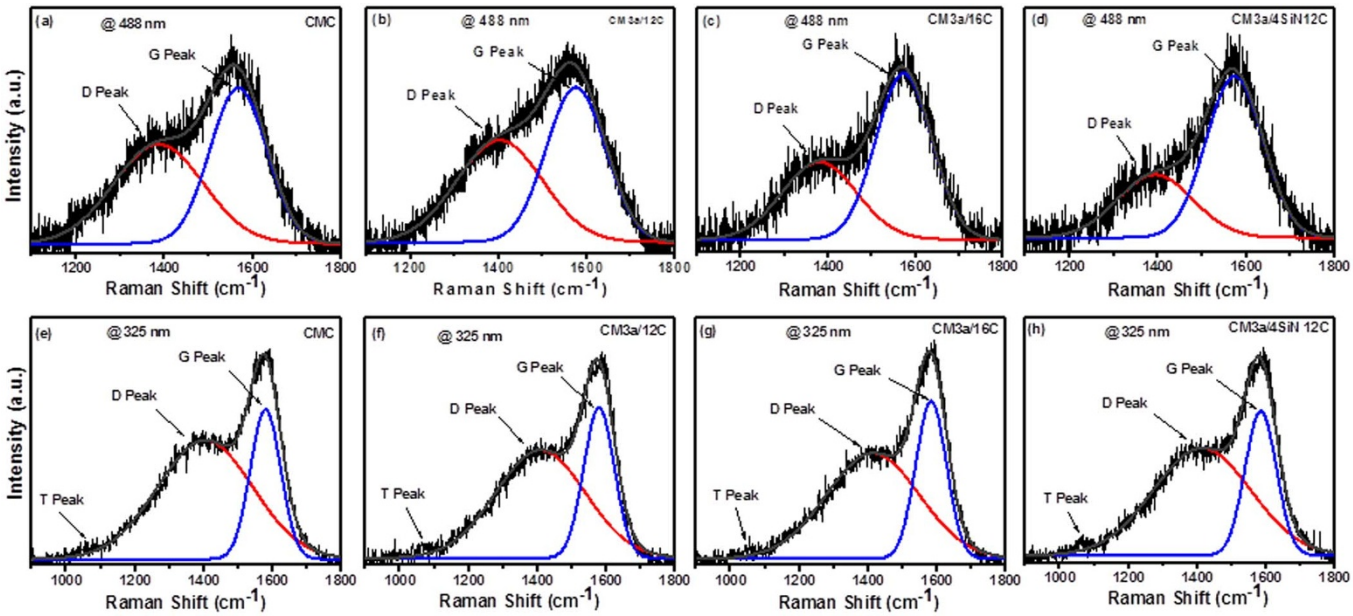

Figure 7 | Visible and UV Raman analyses of the samples. Fitted (a)–(d) visible Raman and (e)–(h) UV Raman spectra of samples CMC, CM3a/12C, CM3a/16C and CM3a/4SiN12C.

with two Gaussian components. The visible Raman spectra showed two bands centered in the range of ~1565–1580 cm^{-1} (G band) and ~1380–1405 cm^{-1} (D band). However, when excited with UV light, the Raman spectra showed an additional band centered in the range of ~1050–1100 cm^{-1} (T band), in addition to the D and G bands centered in the range of ~1400–1420 cm^{-1} and 1580–1590 cm^{-1}, respectively. The G peak corresponds to the symmetrical E_{2g} vibrational mode in graphite-like sp^2 material and arises from the bond stretching motion of all pairs of sp^2 atoms in both rings and chains against the restoring force[34]. The D peak corresponds to the A_{1g} breathing mode of phonons near the zone boundary and appears in the presence of disorder caused by sp^2 atoms in the rings[35]. Hence, both D and G peaks are associated with sp^2C bonding. On the other hand, the T peak which appears in UV excitation can be used for probing sp^3C bonding. Since the T peak in UV excitation was significantly less intense, we could not fit this peak in the Raman spectra.

For the visible Raman spectra as shown in Figs. 7a–7d, the exact G peak position in sample CMC was found to be at 1569.0 cm^{-1}. However, the G peak position in the FCVA-deposited carbon samples CM3a/12C, CM3a/16C and CM3a/4SiN12C was found to be at 1575 ± 1 cm^{-1}. In contrast, the G peak positions in samples CMC, CM3a/12C, CM3a/16C and CM3a/4SiN12C were found to be at 1582.0 cm^{-1}, 1582.0 cm^{-1}, 1586.0 cm^{-1} and 1588.0 cm^{-1}, respectively, in the UV Raman spectra (Figs 7e–7h). Robertson[4] has reported that CH_x films with ~30% sp^3C bonding show a G peak close to 1570 cm^{-1} in visible Raman spectra. In the present case, sample CMC with CH_x OC by PECVD showed a G peak at 1569 cm^{-1} during visible excitation and possessed sp^3C fraction of ~33% (by ARXPS), corroborating with Robertson's results[4]. For the present FCVA-deposited carbon films, the visible Raman spectra showed that the G peaks were almost at the same position. However, the UV Raman spectra showed a gradual shift in the G peak position from 1582 cm^{-1} to 1586 cm^{-1} to 1588 cm^{-1} for samples CM3a/12C, CM3a/16C and CM3a/4SiN12C, respectively. Ferrari and Robertson[34] suggested that for FCVA-deposited carbon films undergoing UV excitation, an increase in the G peak position towards higher wavenumbers corresponds to an increase in sp^3C bonding. Hence, following the model by Ferrari and Robertson[34] and our ARXPS results, it can be concluded that the carbon film on CM3a/4SiN12C contained the highest sp^3C bonding among all the samples. The I_D/I_G ratio, which is related to sp^2 clustering, was also estimated and found to be 0.6, 0.7, 0.5 and 0.4 in samples CMC, CM3a/12C, CM3a/16C and CM3a/4SiN12C respectively, for visible excitation. No significant difference in the I_D/I_G ratio was observed among the samples for UV excitation, which varied between 0.7 and 0.8. This is due to the fact that visible Raman is predominantly sensitive to sp^2C bonding and clustering, whereas the UV Raman signal contains information about sp^3C bonding, in addition to sp^2C bonding. Therefore, the observed change in the G peak positions and I_D/I_G ratios can be attributed to the change in the micro-structure of OCs in terms of sp^3C and sp^2C bonding, sp^2 clustering, their domain size and interfacial bonding, etc. In addition, a small T peak was visible in the UV Raman spectrum of sample CM3a/4SiN12C, as seen in Fig. 7h. This peak was slightly more intense than those for the other samples (Figs. 7e–7g) due to the presence of comparatively more sp^3C bonding, which has also been confirmed earlier by ARXPS.

Discussion

High sp^3C bonding – which improves the wear resistance and density, and enhances the oxidation/corrosion resistance – is the key characteristic of FCVA-deposited carbon films. However, these films show a dramatic change in their structure in terms of loss of sp^3C bonding when the thickness is reduced from bulk to ultrathin film levels. Efforts have been made to maintain/improve the sp^3C bonding, improve the interfacial bonding/strength, and enhance other associated properties by manipulating the structure through the introduction of an atomically thin SiN_x interlayer. In terms of improving interfacial bonding, SiN_x forms two interfaces when sandwiched between the COC and media, namely the upper interface at SiN_x/C and the bottom interface at CoCrPt-Oxide/SiN_x. At the bottom interface, interactions of Co with Si, and Cr with N form Co-Si (silicide) and Cr_2N bonding, respectively. At the top interface, interactions of Si with C, and N with C give rise to strong Si-C and C-N (both sp^2C-N and sp^3C-N) bonding, as confirmed by the ARXPS analysis. Thus, the enhancement in the interfacial bonding with strong bonds, owing to the introduction of the SiN_x interlayer, improves the interfacial strength significantly. These further help to enhance the adhesion of overcoat with underlying media and improve the wear resistance and frictional properties. Enhanced

interfacial strength due to the introduction of a relatively thicker Si interlayer (~1 nm) between Co-based media and FCVA-deposited carbon has been reported earlier[21].

Focusing on the sp^3C and sp^2C bonding, while comparing the ~1.2 nm thick FCVA-deposited carbon in CM3a/12C with ~2.7 nm commercial COC in CMC, it was found that both of the carbon films produced the same sp^3C bonding (~33%), possessed ~63% and ~68% respectively of Co-Co bonding (Co in metallic state), and ~76% and ~77% respectively of Cr-Cr bonding (Cr in metallic state). This revealed that despite a ~55% drop in the COC thickness from CMC to CM3a/12C, the FCVA carbon still provided almost similar corrosion/oxidation protection to the magnetic media (which consist mainly of CoCrPt-alloys). In addition, sp^3C bonding and Cr-Cr metallic bonding were increased to 37% and ~79%, respectively in sample CM3a/16C with ~1.6 nm of carbon film but no change in the oxidation level of Co was observed. The most surprising results were seen in the case of the CM3a/4SiN12C sample when a SiN_x interlayer was introduced. It showed the highest sp^3C bonding of 46.3% among all samples and provided highest oxidation/corrosion resistance to the underlying media layer. The Raman analyses also support the ARXPS results and together, they indicate that the introduction of the SiN_x interlayer promotes (suppresses) sp^3C (sp^2C) bonding. The improved oxidation resistance of sample CM3a/4SiN12C was mainly attributed to the increased sp^3C bonding within the carbon layer, but atomically thin SiN_x interlayer may also have some contribution in protecting the underlying media from oxidation.

Interestingly, while analyzing the I_D/I_G ratio extracted from visible Raman spectra (488 nm), we also observed the influence of thickness and SiN_x interlayer in changing the structural ordering/disordering within the carbon layer of different overcoats. The I_D/I_G ratio is the measure of sp^2 clustering and the formation of number of aromatic rings within the clusters[12,34]. The I_D/I_G ratio varies directly with sp^2 cluster size and the number of aromatic rings. As shown by higher I_D/I_G ratio (0.7), the thinner FCVA deposited carbon such as 1.2 nm COC in sample CM3a/12C had tendency to form a significant amount of aromatic rings and sp^2 clusters, and at the same time showed larger sized sp^2 clusters within the sp^2 and sp^3 bonded carbon system. However, when the thickness of COC was increased to 1.6 nm in sample CM3a/16C, the I_D/I_G ratio decreased to 0.5, suggesting that an increase in thickness prevented the sp^2 clustering and aromatic ring formation, and lowered the size of sp^2 clusters. However, when the atomically thin 0.4 nm SiN_x interlayer was deposited below the 1.2 nm thick COC, the I_D/I_G ratio in sample CM3a/4SiN12C was further reduced to 0.4, indicating that the SiN_x interlayer has a great role in lowering the size of sp^2 clusters and preventing the formation of aromatic rings and sp^2 clusters within the sp^2 and sp^3 bonded carbon network. We have also recorded Raman spectra of these samples using 514 nm excitation to examine the nature of sp^2 clustering and found similar trend as observed with 488 nm excitation (see Supplementary section S3). Overall, the introduction of a SiN_x interlayer below the COC was found to increase the sp^3C bonding, lower the size of sp^2 clusters and decrease the amount and number of aromatic rings and sp^2 clustering within the carbon layer.

Why does an atomically thin SiN_x interlayer help in maintaining/improving sp^3C bonding? To understand this, we discuss the growth mechanism of FCVA-deposited carbon on media samples. In samples CM3a/12C and CM3a/16C, carbon is deposited directly over the CoCrPt:Oxide-media layer. It should be noted that the introduction of metals in DLC films promotes sp^2C bonding[35–37]. Tristsaris *et al.*[38] performed a detailed theoretical study on metal incorporated DLC films and found that the introduction of metals promotes sp^2C bonding mainly at the metal/carbon interface. Both Co and Pt are the transition metals having high adsorption characteristics and are considered as excellent catalysts. As evidence of this, recently, Pohl *et al.*[39] performed a study on FePt/carbon interfaces and found that FePt catalyzed the formation of carbon nanotubes (CNTs), which

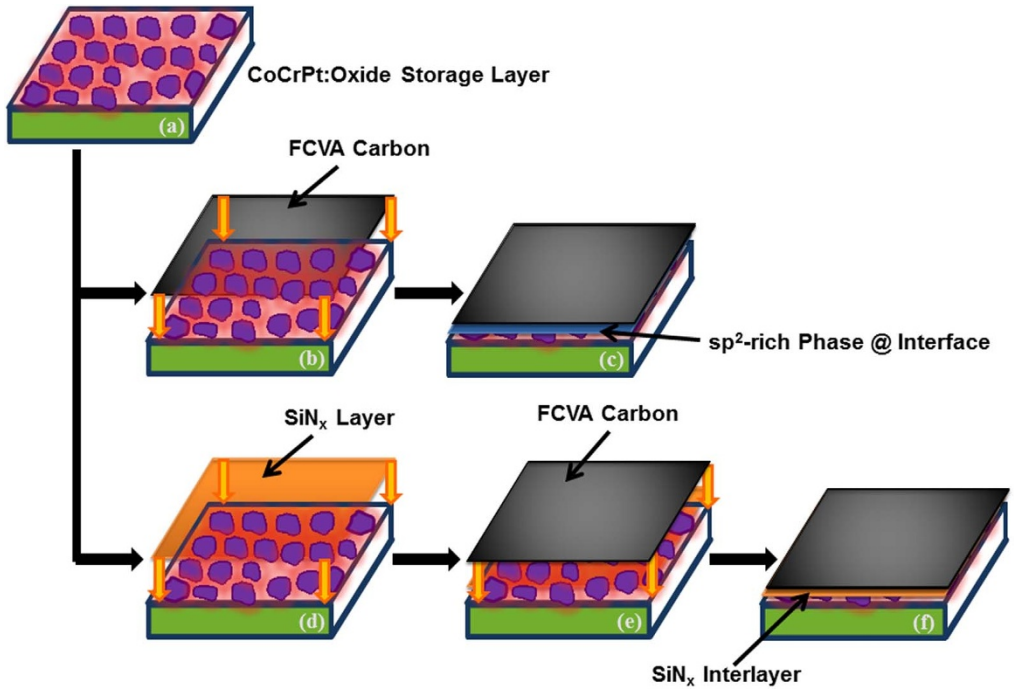

Figure 8 | Schematic illustration of catalytic effect of Co and Pt on interfacial carbon, and how the catalyst effect becomes reduced upon the introduction of an atomically thin SiN_x interlayer. (a) Granular CoCrPt:Oxide storage layer, (b) direct deposition of ultrathin carbon film (in grey color) on the granular media by FCVA, and (c) generation of sp^2-rich interfacial carbon layer (in blue color) due to the catalytic influence of Co and Pt atoms. Figure (d) shows the deposition of a 0.4 nm SiN_x layer (in orange color) on the granular media followed by (e) deposition of an ultrathin carbon film by FCVA. The application of the SiN_x interlayer prevents the catalytic effect on FCVA-deposited carbon at the interface (f) and maintains/improves its sp^3 bonding.

have the sp^2 bonded structure. Bethune *et al.*[40] also reported that Co catalyzed the formation of sp^2 bonded graphite-like structures around the Co clusters. In our case, since the 1.2 nm and 1.6 nm carbon films were extremely thin (comprising just a few atomic layers), we expect the direct interaction of FCVA-deposited carbon with Co and Pt in the media, which promotes sp^2C bonding mainly at the interface region due to the catalytic effect. Moreover, by analyzing the TEM images, we observed the formation of a nano-crystalline layered structure in the CM3a/12C sample, which may be rich in the sp^2 phase mainly at the interface[35–40]. This explains why a lower sp^3C bonding with a fraction of ~33% was observed in sample CM3a/12C. When the thickness of FCVA-deposited carbon was slightly increased to 1.6 nm, the interfacial thickness remained similar, creating the same amount of sp^2C bonding but the bulk thickness increased by ~0.4 nm. This explains why a slightly higher sp^3C bonding of ~37% was observed in CM3a/16C. The catalytic nature of Co and Pt arises from the fact that FCVA-based carbon ions with energy of ~20–25 eV considerably raise the local temperature, referred to as localized heating, upon bombardment onto the CoCrPt-Oxide-media layer. At the same time, Co and Pt atoms lying at the media/carbon interface reduce the activation energy for chemical reactions to be occurring that promote the sp^2 phase of carbon without affecting the total energy required for the product. Hence, amorphous carbon when reacting with Co and Pt atoms transform into the sp^2-rich phase at relatively low temperatures. Weismental *et al.*[41] suggested that carbon ions with energy of 100 eV can heat up a region of 0.75 nm to a local temperature of ~3823 K. The carbon ion energy of 20–25 eV is also sufficient to heat up the substrate locally[33]. Following this assumption, it is possible for the catalytic effect in our case to reach up to ~30–40% of the total film thickness. Thus this region, which can be referred to as the active carbon region, could experience higher sp^2C bonding and clustering.

However, when the SiN_x interlayer was introduced between the 1.2 nm FCVA-deposited carbon film and the CoCrPt-Oxide-media layer, the sp^2C bonding decreased to 29.6%, leading to drastic enhancement of the sp^3C bonding (33% in CM3a/12C versus 46.3% in CM3a/4SiN12C). This can be attributed to the fact that the SiN_x interlayer acts as a "barrier" between the carbon and CoCrPt-Oxide layers, preventing the direct interaction of carbon with either Co or Pt to some extent. Upon carbon ion bombardment, the SiN_x interlayer gives rise to the formation of strong carbide and nitride phases such as SiC and C-N at the upper interface, and Cr_2N and Co-Si silicide bond formation at the bottom interface. Hence, the creation of a "barrier" and the development of strong interfacial bonding at both interfaces owing to the introduction of a SiN_x interlayer reduce the metal-induced transformation of $sp^3 \rightarrow sp^2$ bonding. The schematic view of the Co- and Pt-induced catalytic effect on FCVA-deposited carbon, and how the SiN_x interlayer minimizes the degradation of sp^3C bonding are illustrated in Fig. 8. We also predict that the introduction of the SiN_x interlayer might increase stress at the interface due to an interfacial mismatch between the carbon atoms and Si[42], which is confirmed by the shift of the G peak towards higher wavenumbers during the UV Raman analysis of these samples[43]. Friedman and Sullivan[44] as well as Wang and Komvopoulos[20] have also reported that the interaction of carbon ions with silicon can increase the compressive stress at the Si/C interface. Thus, the increase in stress, to some extent, imposes pressure on the system to lower the Gibbs free energy of sp^3C bonding and hence, this could have led to the increase in sp^3C bonding in sample CM3a/4SiN12C[45]. We also performed tribological and electrochemical corrosion measurements on these samples and results are reported in supplementary information (Supplementary Figs. S2.1, S2.2 and S2.3). We observed that sample CM3a/4SiN12C performed well in terms of having high wear resistance, a lower coefficient of friction and high oxidation/corrosion resistance as compared to the other FCVA-deposited COCs and commercial COC. This could be due to the SiN_x-induced strong interfacial bonding and improved sp^3C bonding of carbon films.

In summary, by introducing an atomically thin SiN_x interlayer to the designed overcoat structure, we have been able to maintain/increase the sp^3C bonding, improve the adhesion of overcoat with underlying media and maintain/improve other associated properties of ultrathin carbon films such as low friction, high wear and oxidation/corrosion resistance. These findings are extremely important towards the realization of thin yet protective overcoats for high density magnetic storage media.

Methods

Sample fabrication. For comparison and investigation, five different types of samples were included in the present work, as described in Table 1. Sample CMb was bare magnetic media with neither COC nor lube, and CMC was commercial media with commercial COC (~2.7 nm) but without lube. The deposition of carbon films for CM3a/12C, CM3a/16C and CM3a/4SiN12C was performed *in-situ* on etched CM3a media by FCVA (Veeco Instrument Inc.) at carbon ion energy of ~20–25 eV (without intentional substrate biasing). The FCVA system was equipped with single 90° bend filter and high current pulsed power supply. During deposition of carbon by FCVA, pulsed power was applied to the target. Prior to final deposition, the calibration of the deposition rate was performed using XRR technique. We have calibrated the deposition thickness as a function of number of pulses applied to the target. The deposition rate calibrated by XRR was found to be ~0.063 Å/pulse. By adjusting the number of pulses, the samples with desired carbon thicknesses were prepared. Further, in sample CM3a/4SiN12C, the SiN_x interlayer (0.4 nm) was deposited by pulsed DC reactive sputtering.

Characterizations. The thicknesses of the OCs, in cross-section geometry, were measured by high resolution TEM (Philips CM300 FEG). The samples for TEM imaging were prepared in various steps. ARXPS measurements (VG ESCALAB 220I-XL) were performed in an ultrahigh vacuum (~10^{-9} Torr) with varying TOA from 15° to 65°.The monochromatic Al K_α was used as the X-ray source (1486.6 eV). The micro-Raman measurements were performed with a Jobin Yvon LABRAM-HR set-up. An excitation wavelength of 488 nm from an Ar laser was used for visible Raman while an excitation wavelength of 325 nm from a He-Cd laser was used for UV Raman measurements. The spot size was fixed at ~1 μm for the analysis.

1. Casiraghi, C., Robertson, J. & Ferrari, A. C. Diamond-like carbon for magnetic data and beer storage. *Mater. Today* **10**, 44–53 (2007).
2. Zhang, H. S. & Komvopoulos, K. Surface modification of magnetic recording media by filtered cathodic vacuum arc. *J. Appl. Phys.* **106**, 093504 (2009).
3. Casiraghi, C. *et al.* Ultra-thin carbon layer for high density magnetic storage devices. *Diamond Relat. Mater.* **13**, 1480–1485 (2004).
4. Robertson, J. Requirements of ultrathin carbon coatings for magnetic storage technology. *Tribol. Int.* **36**, 405–415 (2003).
5. Gaur, N. *et al.* Lateral displacement induced disorder in L10-FePt nanostructures by ion-implantation. *Sci. Rep.* **3**, 1907 (2013).
6. Marchon, B., Pitchford, T., Hsia, Y. T. & Gangopadhyay, S. The head-disk interface roadmap to an areal density of 4 Tb/in^2. *Adv. Tribol.* **2013**, 521086 (2013).
7. Wallace, R. L. The reproduction of magnetically recorded signals. *Bell Syst. Tech. J.* **30**, 1145–1173 (1951).
8. Wang, N., Komvopoulos, K., Rose, F. & Marchon, B. Structural stability of hydrogenated amorphous carbon overcoats used in heat-assisted magnetic recording investigated by rapid thermal annealing. *J. Appl. Phys.* **113**, 083517 (2013).
9. Pathem, B. K. *et al.* Carbon overcoat oxidation in heat-assisted magnetic recording. *IEEE Trans. Magn.* **49**, 3721–3724 (2013).
10. Bhatia, C. S. *et al.* Ultrathin overcoat for the head/disk interface tribology. *J. Tribol.* **120**, 795–799 (1998).
11. Samad, M. A. *et al.* A novel approach of carbon embedding in magnetic media for future head/disk interface. *IEEE Trans. Mag.* **48**, 1807–1812 (2011).
12. Chhowalla, M., Ferrari, A. C., Robertson, J. & Amaratunga, G. A. J. Evaluation of sp^2 bonding with deposition temperature in tetrahedral amorphous carbon studied by Raman spectroscopy. *Appl. Phys. Lett.* **76**, 1419–1421 (2000).
13. Beghi, M. G. *et al.* Bonding and mechanical properties of ultrathin diamond-like carbon films. *Appl. Phys. Lett.* **81**, 3804–3806 (2002).
14. Ferrari, A. C. Diamond-like carbon for magnetic storage disks. *Surf. Coat. Technol.* **180-181**, 190–206 (2004).
15. Rose, F. *et al.* Low surface energy and corrosion resistant ultrathin TiSiC disk overcoat. *J. Appl. Phys.* **113**, 213513 (2013).
16. Rose, F. *et al.* Ultrathin TiSiN overcoat protection layer for magnetic media. *J. Vac. Sci. Technol. A* **29**, 051501 (2011).
17. Bunnak, P., Gong, Y., Limsuwan, S., Pokaipisit, A. & Limsuwan, P. Chemical bonding in composite SiN_x/diamond-like carbon films prepared by filtered cathodic vacuum arc deposition of graphite incorporated with radio frequency sputtering of silicon nitride. *Jpn. J. Appl. Phys.* **52**, 095501 (2013).

18. Bunnak, P., Gong, Y., Limsuwan, S., Pokaipisit, A. & Limsuwan, P. Mechanical properties of composite SiN_x/diamond-like carbon films prepared by filtered cathodic vacuum arc deposition of graphite incorporated with radio frequency sputtering of silicon nitride. *Mater. Sci. Appl.* **4**, 564–571 (2013).
19. Zhang, H. S. & Komvopoulos, K. Synthesis of ultrathin carbon films by direct current filtered cathodic vacuum arc. *J. Appl. Phys.* **105**, 083305 (2009).
20. Wang, N. & Komvopoulos, K. Incidence angle effect of energetic carbon ions on deposition rate, topography, and structure of ultrathin amorphous carbon films deposited by filtered cathodic vacuum arc. *IEEE Trans. Mag.* **48**, 2220–2227.
21. Rismani, E. *et al.* Ultrathin Si/C graded layer to improve tribological properties of Co magnetic films. *Appl. Phys. Lett.* **101**, 191601 (2012).
22. Biesinger, M. C. *et al.* Resolving surface chemical states in XPS analysis of first row transition metals, oxide and hydroxides: Cr, Mn, Fe, Co and Ni. *Appl. Surf. Sci.* **257**, 2717–2730 (2011).
23. Petitto, S. C., Marsh, E. M., Carson, G. A. & Langell, M. A. Cobalt oxide surface chemistry: The interaction of CoO (1000), Co_3O_4 (110) and Co_3O_4 (111) with oxygen and water. *J. Mol. Catal. A: Chem.* **281**, 49–58 (2008).
24. Wagner, C. D., Riggs, W. M., Davis, L. E., Moulder, J. F. & Muilenberg, G. E. *Handbook of X-ray photo-electron spectroscopy*. [1–190] (Perkin-Elmer Corporation, 1979).
25. Prabhakaran, K. & Ogino, T. Behaviour of ultrathin layers of Co on Si and Ge. *Appl. Surf. Sci.* **100–101**, 518–521 (1996).
26. Stypula, B. & Stoch, J. The characterization of passive films on chromium electrodes by XPS. *Corros. Sci.* **36**, 2159–2167 (1994).
27. Lu, C. E., Pu, N. W., Hou, K. H., Tseng, C. C. & Ger, M. D. The effect of formic acid concentration on the conductivity and corrosion resistance of chromium carbide coatings electroplated with trivalent chromium. *Appl. Surf. Sci.* **282**, 544–551 (2013).
28. Jiang, T., Wallinder, I. O. & Herting, G. Chemical stability of chromium carbide and chromium nitride powders compared with chromium metal in synthetic biological solutions. *ISRN Corros.* **2012**, 379697 (2012).
29. Matsuoka, M., Isotani, S., Sucasaire, W., Zambom, L. S. & Ogata, K. Chemical bonding and composition of silicon nitride films prepared by inductively coupled plasma chemical vapor deposition. *Surf. Coat. Technol.* **204**, 2923–2927 (2010).
30. McCann, R. *et al.* Chemical bonding modifications of tetrahedral amorphous carbon films induced by rapid thermal annealing. *Thin Solid Films* **482**, 34–40 (2005).
31. Yan, X. *et al.* Preparation and characterization of electrochemically deposited carbon nitride films on silicon substrate. *J. Phys. D Appl. Phys.* **37**, 1–7 (2004).
32. Geppert, I., Lipp, E., Berner, R., Hung, S. & Eizenberg, M. Effect of composition and chemical bonding on the band gap and band offsets to Si of $Hf_xSi_{1-x}O_2$ (N) films. *J. Appl. Phys.* **107**, 053701 (2010).
33. Feng, W. J. *et al.* Structural and magnetic properties of Cr(N)-β-Cr2N nanoparticles prepared by arc discharge. *J. Alloys Compd.* **425**, 4–9 (2006).
34. Ferrari, A. C. & Robertson, J. Resonant Raman spectroscopy of disordered, amorphous, and diamond-like carbon. *Phys. Rev. B* **64**, 075414 (2001).
35. Dwivedi, N. *et al.* Influence of silver incorporation on the structural and electrical properties of diamond-like carbon thin films. *ACS Appl. Mater. Interfaces* **5**, 2725–2732 (2013).
36. Lee, C. S., Kim, T. Y., Lee, K. R. & Yoon, K. H. Nanoscale manipulation of tetrahedral amorphous carbon films. *Thin Solid Films* **447–448**, 169–173 (2004).
37. Khun, N. W., Liu, E. W., Yang, G. C., Ma, W. G. & Jiang, S. P. Structure and corrosion behavior of platinum/ruthenium/nitrogen doped diamond-like carbon thin films. *J. Appl. Phys.* **106**, 013506 (2009).
38. Tritsaris, G. A., Mathioudakis, C., Kelires, P. C. & Kaxiras, E. Optical and elastic properties of diamond-like carbon with metallic inclusions: A theoretical study. *J. Appl. Phys.* **112**, 103503 (2012).
39. Pohl, D. *et al.* Understanding the metal-carbon interface in FePt catalyzed carbon nanotubes. *Phys. Rev. Lett.* **107**, 185501 (2011).
40. Bethune, D. S. *et al.* Cobalt catalyzed growth of carbon nanotubes with single-atomic-layer walls. *Nature* **363**, 605–607 (1993).
41. Weissmantel, C. *et al.* Structure and properties of quasi-amorphous films prepared by ion beam techniques. *Thin Solid Films* **72**, 19–31 (1980).
42. Han, X., Zhu, J., Han, J., Tan, M. & Gao, W. Stress, microstructure and mechanical properties of graded multilayer tetrahedral amorphous carbon films. *Appl. Phys. A* **91**, 529–533 (2008).
43. Shin, J. K., Lee, C. S., Lee, K. R. & Eun, K. Y. Effect of residual stress on the Raman spectrum analysis of the tetrahedral amorphous carbon films. *Appl. Phys. Lett.* **78**, 631–633 (2001).
44. Friedmann, T. A. & Sullivan, *Research Briefs* published by Physical, Chemical, and Nano Sciences Center, Sandia National Laboratories, 70–71 (2007) (Date of access: 31/01/2014) http://www.sandia.gov/pcnsc/research/researchbriefs/2007.
45. McKenzie, D. R., Muller, D. & Pailthorpe, B. A. Compressive-stress-induced formation of thin film tetrahedral amorphous carbon. *Phys. Rev. Lett.* **67**, 773–776 (1991).

Acknowledgments

This research is supported by the National Research Foundation, Prime Minister's Office, Singapore under its Competitive Research Programme (CRP Award No. NRF-CRP 4-2008-06).

Author contributions

N.D., E.R., R.J.Y., P.S.G., N.S., S.N., B.D., S.T. performed experiments. N.D. and C.S.B. analyzed the data. N.D. and C.S.B. wrote the main manuscript text and prepared figures. All authors reviewed the manuscript.

Additional information

Supplementary information accompanies this paper at http://www.nature.com/scientificreports

Competing financial interests: The authors declare no competing financial interests.

How to cite this article: Dwivedi, N. *et al.* Probing the Role of an Atomically Thin SiN_x Interlayer on the Structure of Ultrathin Carbon Films. *Sci. Rep.* **4**, 5021; DOI:10.1038/srep05021 (2014).